# Estimating Bowen Index in urban environment based on Landsat 8/9 imagery

Tereza Pohanková[1] and Vilém Pechanec[1]

[1]Department of geoinformatics, Palacky University Olomouc, Czechia

**Correspondence:** Tereza Pohanková (tereza.pohankova@upol.cz)

**Abstract.** This study explores the Olomouc region's thermal dynamics and energy balance in northeastern Czech Republic during the spring and summer of 2022. Using Landsat 8 and Landsat 9 imagery, meteorological data and the S-SEBI model to determine Bowen Index (BI). Analysis of Solar Net Radiation and Sensible and Latent Heat Fluxes contributes to our understanding of energy exchanges at the surface. The S-SEBI algorithm helps determine Bowen Index, highlighting patterns

5   across land cover classes. Urban and artificial areas consistently exhibit higher Bowen Index values, suggesting a higher sensible heat flux. Areas with vegetation showcase lower BI values, indicating the dominance of latent heat flux and the cooling effect of vegetation. Temporal trends in BI vary during specific sensing days. Despite challenges associated with atmospheric variability, our integration of meteorological data and remote sensing techniques contributes to understanding the local climate. Validation with EUMETSAT evaluation data indicates a consistent relationship with some biases, implying

10   Potential reliability of our approach and the derived heat fluxes and Bowen Index values.

## 1 Introduction

The Bowen ratio ($\beta$ or BI) is a crucial physical metric capturing the dynamics of land surface climate. It provides a comprehensive overview of how microclimate and hydrological processes intricately shape ecosystem energy distribution and influence water utilization. Previous research on land-atmosphere interactions has consistently highlighted the pivotal role of $\beta$, empha-

15   sizing its significance in unravelling the complexities inherent in these ecological processes (Cho et al., 2012). As Wilson et al. (2002) stated even during stable season the values of Bowen Index may significantly vary.

Although various studies regarding Bowen Index have been published, there are not many of them. Scopus database records 258 results (the first one published in 1994) *Bowen Index* but only 60 are included with second key word *Remote Sensing*. Word of Science database knows of 1 900 studies (the first one from 1992) of the Bowen Index, but only 144 are connected with

20   *Remote Sensing*. Bowen Index, along with Eddy Covariance, is one of the most popular-field based methods for estimating information regarding evapotranspiration (Chatterjee et al., 2023).

Estimates of Bowen Index variables are needed on both local and global scales. While on a global scale we can find several products ready for analysis, this is often not the case for regional and local needs (especially due to coarse spatial resolution). Meteorological methods such as Bowen Ratio Energy Balance (Held et al., 1990) or Eddy Covariance (Law et al., 2002) require

25   a lot of in-situ data. However, these methods only allow us to conduct our analyses on point data, while a spatial view is needed

for deeper understanding and more precise predictions. While several meteorological approaches, such as Eddy Covariance, are able to work on a larger scale and enable us for spatial analyzing (up to approximately 100 $km^2$), the cost is too high for frequent and repetitive usage (Anderson and Goulden, 2009).

30  This paper describes estimating Bowen Index through remotely sensed Landsat 8 and Landsat 9 satellite images supplemented with meteorological data acquired in situ. Sensible and Latent Heat Flux, needed to determine the Bowen Index, were calculated through the S-SEBI algorithm (Roerink et al., 2000).

This study's innovative approach to Bowen Index in this study lies in its application as a remotely sensed variable, deviating from the conventional approach of relying solely on in-situ measuring towers. While various meteorological markers such as Albedo (Liang, 2001), Land Surface Temperature Avdan and Jovanovska (2016), and Heat Fluxes Heat Fluxes (Berbers and
35  Zwaenepoel, 2021) are routinely derived from remotely sensed data, the Bowen Index stands out for its utilization in revealing spatial distribution patterns (Nagler et al., 2005) (Mallick et al., 2009) (Wylie et al., 2003). This departure from the traditional reliance on ground-based measurements underscores its significance as a valuable meteorological parameter, particularly when exploring large-scale phenomena. When harnessed as a remotely sensed variable, the Bowen Index offers a unique perspective on spatial dynamics, making it an indispensable tool in understanding and analyzing the intricate interplay of environmental
40  factors.

## 2 Study area

The solution is applied in a real environment in a typical Central European landscape. The urban environment is composed of a mosaic of natural, near-natural, and completely artificial surfaces. The average size of individual patches is highly variable.

The region of interest covers Olomouc, the regional capital city (the sixth largest city in the Czech Republic with approxi-
45  mately one hundred citizens), covering approximately 103.230 $km^2$ located in the northeastern path of the Czech Republic in the historical region of Moravia (see Fig. 1).The city houses the second-oldest university in the Czech Republic and the oldest in Moravia (University, 2024).

The climate is affected by its continental conditions. Annual rainfall is approximately between 600 mm to 1000 mm. The river Moravia goes through the city from north to south direction, Olomouc being the largest city situated directly on its banks.
50  Land cover differs through the region (see Fig. 3). The urban and suburban parts are located in the centre. The further from the centre, the more rural land cover, with mixed forest types in the northeastern parts (ČÚZK et al., 2023).

**Figure 1.** Localization of area of interest.

## 3 Methodology

### 3.1 Data sources

Landsat 8 and Landsat 9 imagery were downloaded from the Earth Explorer, the United States Geological Survey website

55 (http://earthexplorer.usgs.gov) over spring and summer of 2022 (May to August) for paths 189 and 190 and rows 025 and 026. Optimal cloud coverage was assessed visually. Nine sensing days were chosen for analysis (Table 1). The image levels downloaded were L1TP and L2SP.

**Table 1.** Landsat satellite sensing days.

| Satellite platform | Sensing day | Path | Row |
|---|---|---|---|
| LC09 | 18th May 2022 | 190 | 025 |
| LC08 | 19th May 2022 | 189 | 026 |
| LC09 | 12th June 2022 | 189 | 026 |
| LC08 | 20th June 2022 | 189 | 026 |
| LC08 | 27th June 2022 | 190 | 025 |
| LC09 | 21st July 2022 | 190 | 025 |
| LC08 | 22nd July 2022 | 189 | 026 |
| LC09 | 15th August 2022 | 189 | 026 |
| LC08 | 30th August 2022 | 190 | 025 |

Meteorological data were downloaded from CHMI (Czech Hydro-meteorological Institute) in a CSV (Comma Separated Values) format for each sensing day. Specific variables and their units for can be seen in Table 2.

**Table 2.** Meteorological data used in the study.

| Name | Units | Symbol |
|---|---|---|
| Average Air Temperature | °C | Ta |
| Maximum air temeprature | °C | Ta_max |
| Minimum Air Temperature | °C | Ta_min |
| Wind Speed | m/s | U |
| Relative Air Humidity | % | RH |

60    The study area has been defined by official administrative units used for municipalities (level *obce*) as recognized by the State Administration of Land Surveying and Cadastre (*https://www.cuzk.cz/en*).

The land cover/land use map was created by aggregating a Detailed combined layer of habitats, which CzechGlobe produced on a scale of 1: 10 000 (with the last update in 2019); for details, see Pechanec et al. (2021).Forty-nine habitat classes with various degrees of naturalness covered our area of interest. These 49 unique habitats were then aggregated into six groups based

65    on their eco-physiological properties and scale (habitats smaller than the Landsat 8/9 pixel were merged with the closest habitat larger than the satellite pixel). Six newly aggregated groups (see Table 3 and Fig. 2) were were Agricultural land, Water and Wetlands Tree vegetation, Artificial and Urban fabric, Meadows and grasslands, Other (2) representing actual land cover/land use classes.

**Table 3.** Area of habitat groups.

| LULC class | Area $[km^2]$ | Area [%] |
|---|---|---|
| Agricultural land | 53.912 | 52.2 |
| Water and wetland | 1.860 | 1.9 |
| Tree vegetation | 12.486 | 11.6 |
| Artificial + Urban Fabric | 30.660 | 29.7 |
| Meadow and grassland | 0.672 | 0.6 |
| Other | 3.770 | 4.0 |
| **SUM** | **103.36** | **100** |

### 3.2  Processing

70  All values were calculated from Landsat 8/9 images covering the study area during 2022 (see Table 1). As pre-processing, the data were visually analyzed for remnants of clouds or large shadows. After that, the original tiles were cropped to the area of interest, and relevant meteorological (e.g. Water et al.) and surface (e.g. Vegetation Indices or Surface Emissivity) variables were calculated. The calculation process is shown in Figure 3.

Hydrology and
Earth System
Sciences
Discussions
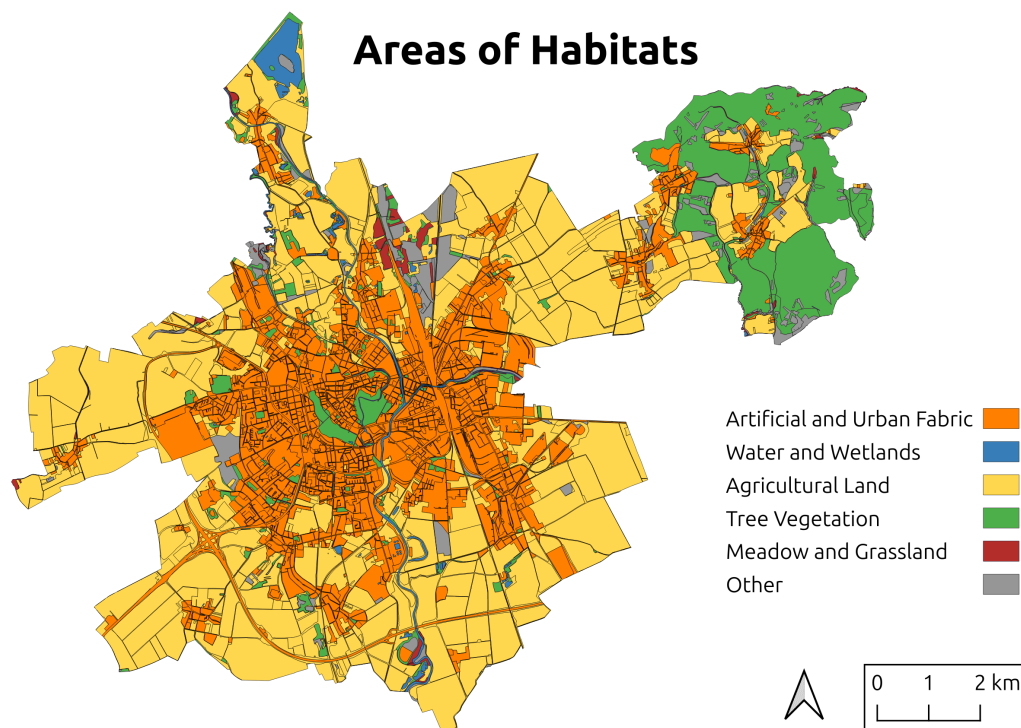


**Figure 2.** Actual land cover/land use map of Olomouc

The processing started with calculating Land Surface Temperature and Albedo, which were then used to calculate Net
75 Radiation and Ground Heat Flux. Sensible and Latent Heat Fluxes were then determined by the S-SEBI (Roerink et al., 2000)
model. S-SEBI uses Evaporative Fraction to determine Sensible and Latent Heat Flux based on two limit pixels (hot and dry).
Lastly, Bowen Index was calculated as a fraction of Sensible and Latent Heat Flux.

### 3.2.1 Land Surface Temperature

The USGS provides the finished LST product directly using the Earth Explorer repository, but the resulting imagery was
80 corrupted in the area of interest for most sensing days. Therefore, LST was calculated separately using the algorithm proposed
by Avdan and Jovanovska (2016).

$$LST = \frac{BT}{1 + (\frac{\lambda \times BT}{\rho}) \times \ln(LSE)} \tag{1}$$

where LST is in Celsius (°C), BT is at-sensor temperature (°C), $\lambda$ and $\rho$ are a constants equal to 10.895 (see Markham and
Barker (1985)) and $1.438 \times 10^{-2}$ respectively (see Weng et al. (2004)) and LSE stands for Land Surface Emissivity.
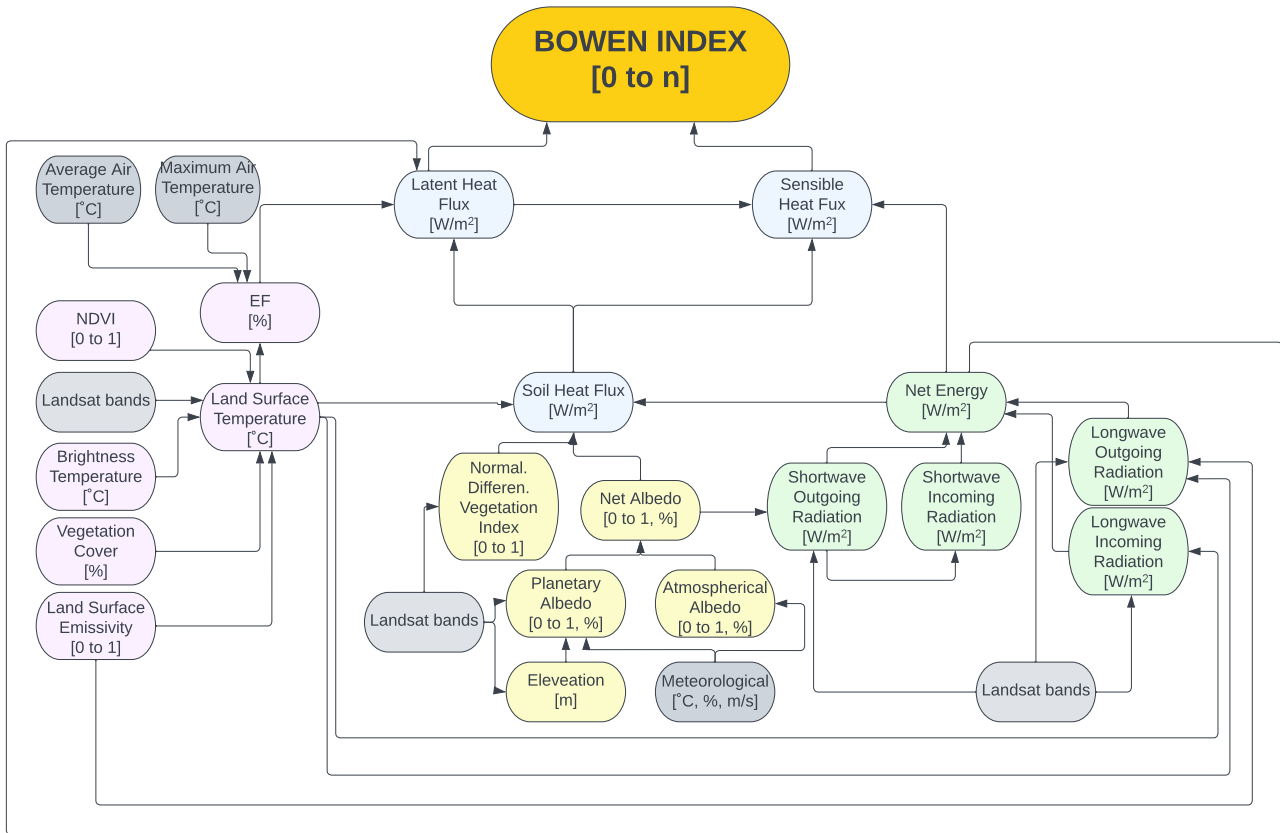
**Figure 3.** Process of Bowen Index calculation.

### 3.2.2 Albedo

Albedo was derived based on an approach by Yale University (https://yceo.yale.edu/how-convert-landsat-dns-albedo) originally proposed by Liang (2001) for Landsat TM/ETM+ (Thematic Mapper/Enhanced Thematic Mapper plus). This method was proven efficient also for new versions of Landsat satellite by Favretto et al. (2018). The equation used for Landsat 8/9 is as follows:

$$\alpha = \frac{0.365 \times \rho_2 + 0.130 \times \rho_4 + 0.373 \times \rho_5 + 0.085 \times \rho_6 + 0.072 \times \rho_7 - 0.0018}{0.356 + 0.130 + 0.373 + 0.0085 + 0.072} \tag{2}$$

where $\rho_x$ stands for respective band of Landsat 8 or Landsat 9.

Hydrology and
Earth System
Sciences
Discussions

Open Access

EGU

### 3.2.3 Net Radiation

Solar net radiation (in $W/m^2$) was estimated using balance of energy between incoming ($R_s \downarrow$; $R_l \downarrow$) and outgoing ($R_s \uparrow$; $R_l \uparrow$) shortwave and longwave radiation fluxes at surface.

95   The net radiation ($R_n$) is obtained by summing up the net surface shortwave ($R_s$) and longwave ($R_l$) radiation as can be seen in Sai Krishna et al. (2014):

$$R_n = R_s + R_l = (R_s \downarrow - \alpha R_s \uparrow) + (R_l \downarrow + R_l \uparrow) \tag{3}$$

### 3.2.4 Determining Heat Fluxes using S-SEBI

Sensible (H) and Latent (LE) Heat Fluxes (in $W/m^2$) were derived using S-SEBI algorithm (Simplified Surface Energy Balance

100   Index) originally designed by Roerink et al. (2000). S-SEBI calculates evaporative fraction which si then used to determine H and LE. However, S-SEBI has a limitation; constant atmospheric conditions are needed over the imagery to distinguish limited pixels properly.

The Evaporative fraction ($\Lambda$) is derived using the three heat fluxes (LE - Latent, H - Sensible and G - Ground). G was calculated separately using the original SEBS formula by Su (2002) with a fraction of vegetation cover $f_c$. In some cases,

105   Ground Heat Flux is approximated as ten percent of total Net Radiation, however, to keep values as accurate as possible, it was calculated using SEBS (Su, 2002).

$$G = R_n \times (0.315 + (1 - f_c) \times (0.05 - 0.315)) \tag{4}$$

$$\Lambda = \frac{LE}{H + LE} = \frac{LE}{R_n - G} \tag{5}$$

in S-SEBI Evaporative Fraction is calculated as follows using the limit pixels:

110   $$\Lambda = \frac{T_h - LST}{T_h - T_c} \tag{6}$$

where $T_h$ is the temperature of hot (dry) pixel and $T_c$ is the temperature of cold (wet) pixel.

As stated by Acharya and Sharma (2021), S-SEBI does not require any meteorological data and is based on the correlation of Land Surface Temperature and albedo. The H and LE can be derived from the evaporative fraction as proposed by Roerink et al. (2000):

115   $$H = (1 - \Lambda) \times (R_n - G) \qquad\qquad LE = \Lambda \times (R_n - G) \tag{7}$$

Hydrology and
Earth System
Sciences
Discussions

Using these fluxes, we can determine the ratio for Bowen Index (BI):

$$BI = \frac{H}{LE} \tag{8}$$

## 4 Results

The application of the method brought several partial intermediate results (of Sensible Heat and Latent Heat Flux) that are
120    entirely new to the area of interest. Sensible and Latent Heat Fluxes, crucial surface energy balance components, were deter-
mined using the S-SEBI algorithm. Urban areas exhibit higher Sensible Heat Flux, indicating a prevalence of heat conduction
and storage (6). In contrast, vegetated areas display higher Latent Heat Flux values (7 and Fig. 4), indicative of the cooling
effect of evapotranspiration.
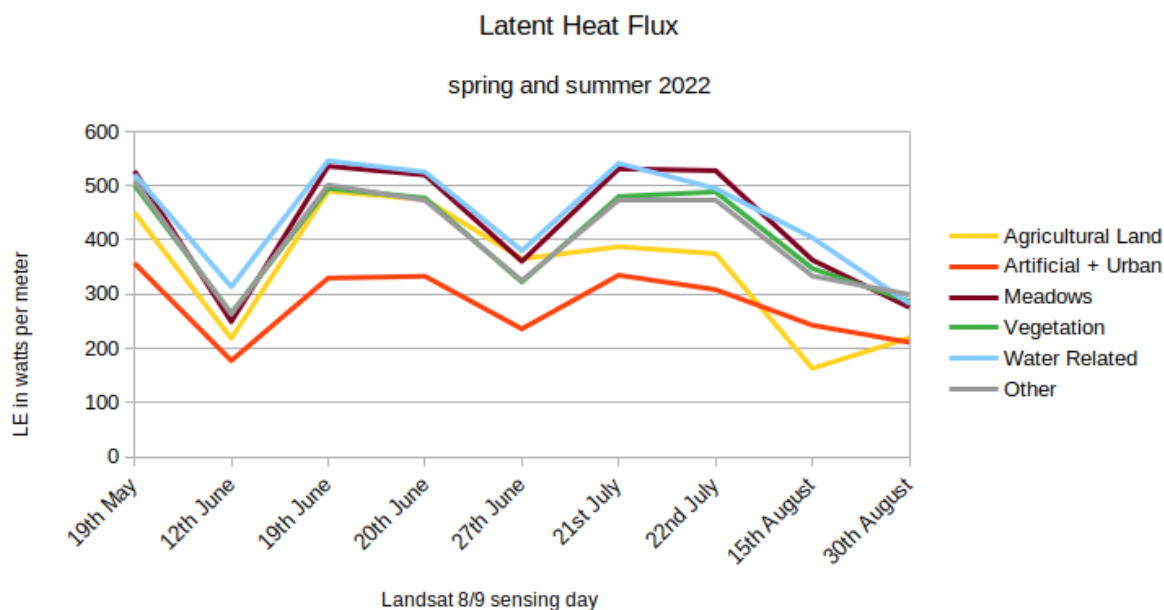


**Figure 4.** Latent Heat Flux Values on areas of habitats through spring and summer 2022.

The calculated values are in the interval from approximately 200 to 600 $W/m^2$ for Sensible Heat Flux and to 130 to 550
125    $W/m^2$ for Latent Heat Flux, whose time course and spatial distribution can be seen in Figures and 5, 6 and 7. The variability
of values reflects the heterogeneity and dominant habitat groups in the area of interest very well.

In general, the magnitudes of LE values appear to be larger compared to the H. The contributions of land cover types to LE
and H can vary. For instance, Meadows and Vegetation contribute significantly to both LE and H. The Water-related group also
shows notable contributions in both cases, while other land cover types may have distinct responses.
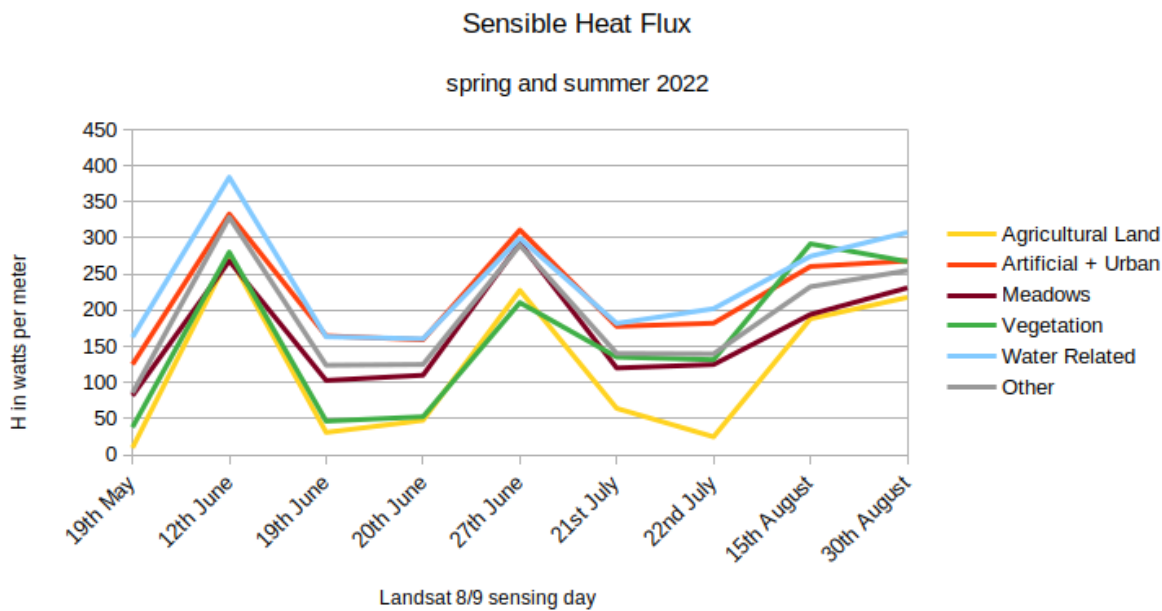
**Figure 5.** Sensible Heat Flux Values on areas of habitats through spring and summer 2022.

130    These components have never been derived in this way for the area of interest. The key benefit, and also valid for further results, is the calculation for the whole region at one point; the data generates a time series that shows spatio-temporal variability at a scale applicable for spatial planning.
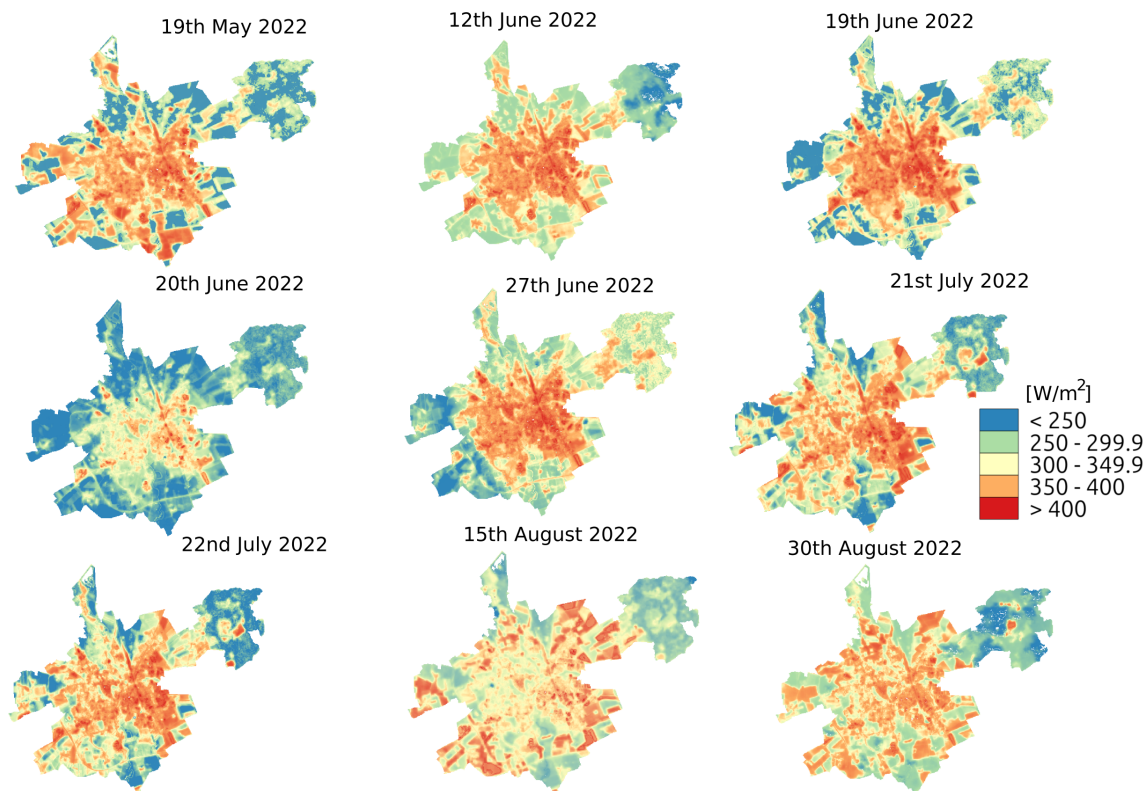
**Figure 6.** Sensible Heat Flux Values through Spring and Summer 2022.

Higher values of sensible heat flux (especially in places with higher LST) contribute to the urban heat island phenomenon. This effect is described by increased temperature in urban environments and environments with impermeable surfaces. A
135   contrast between areas with high sensible and high latent heat flux can be seen throughout the study period.
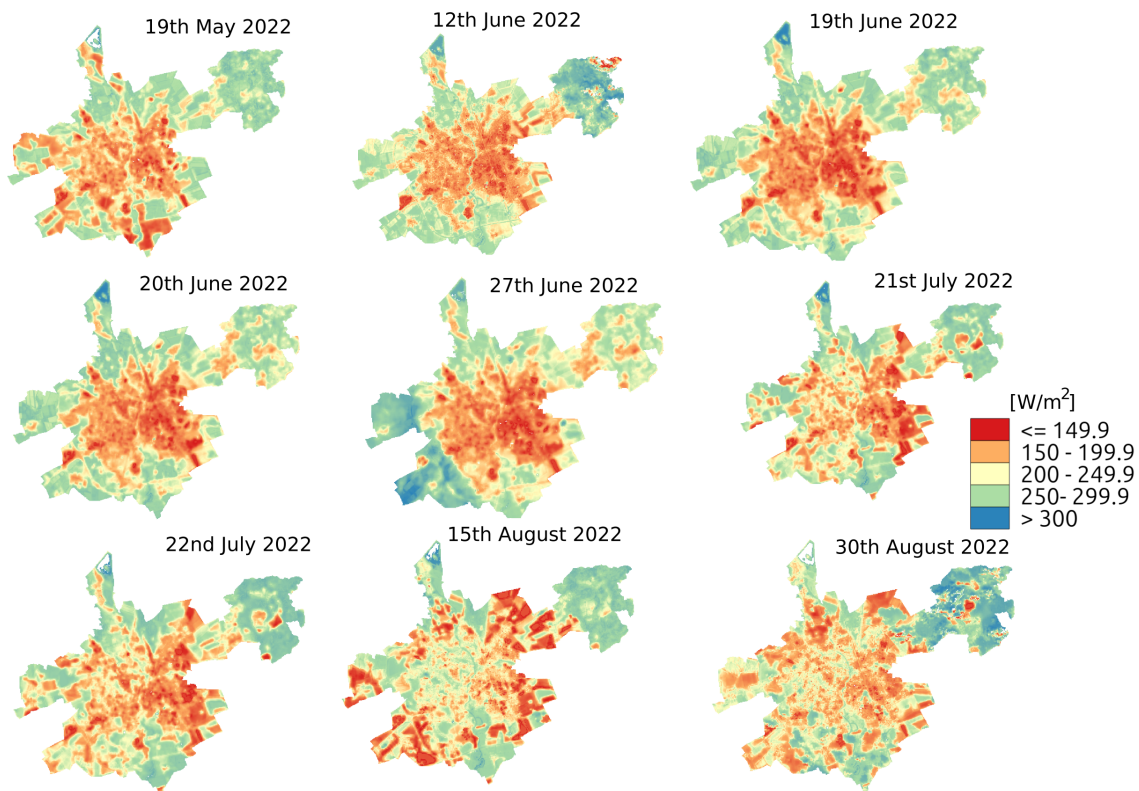
**Figure 7.** Latent Heat Flux Values through Spring and Summer 2022.

## 4.1 Bowen Index

The study's main result is determining Bowen Index for previously created Land Cover classes (Fig. 2) for spring and summer in 2022. The main results are shown in Table 4, where are highlighted minimal (green) and maximum (red) values of Bowen Index.

Hydrology and
Earth System
Sciences
Open Access
EGU
Discussions
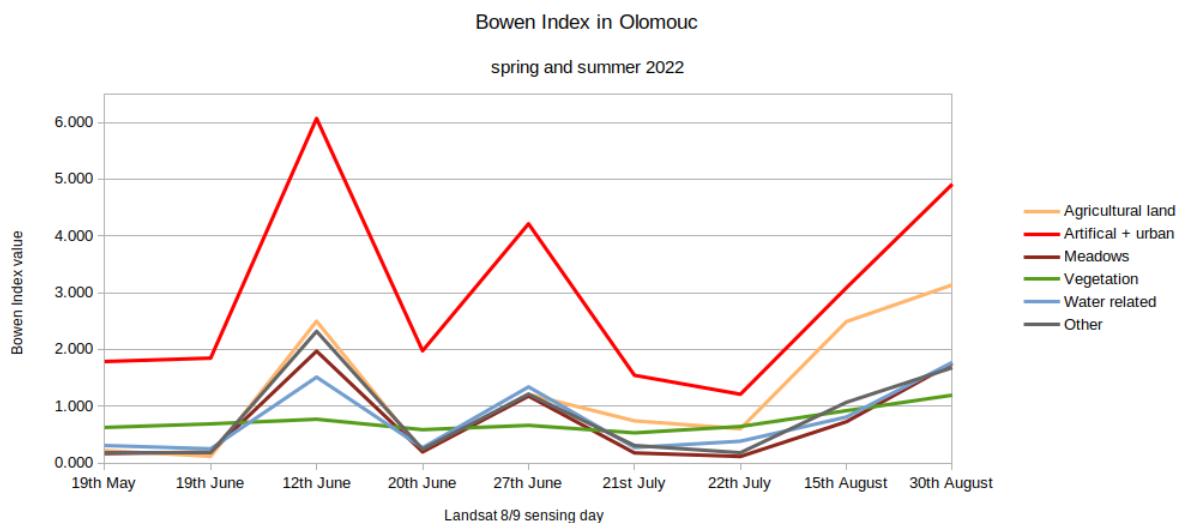
**Figure 8.** Bowen Index Values on areas of habitats through spring and summer 2022.

140    A series of nine maps for each sensing day was created (Fig. 9). Different land classes exhibited Bowen Index patterns, indicating varied contributions to sensible and latent heat fluxes. Urban and artificial areas tended to have higher Bowen Index values, suggesting a dominance of sensible heat flux, especially on specific dates like 12th June and 22nd July 2022. Areas with significant vegetation, such as meadows or forests, tend to have lower Bowen Index values, especially large forests in the northeast of the area of interest. This implies a larger contribution to latent heat flux, reflecting the cooling effect of vegetation

145    through evapotranspiration. The vegetation class also had the most stable trend over the sensing period (see Fig. 8).

**Table 4.** Progress of Bowen Index on areas of habitats.

| Date | 19th May | 19th June | 12th June | 20th June | 27th June | 21st July | 22nd July | 15th Aug. | 30th Aug. |
|---|---|---|---|---|---|---|---|---|---|
| **Class** | | | | | | | | | |
| Agricultural land | 0.217 | 0.117 | 2.496 | 0.187 | 1.207 | 0.741 | 0.602 | 2.490 | 3.317 |
| Other | 0.189 | 0.174 | 2.318 | 0.240 | 1.213 | 0.307 | 0.180 | 1.068 | 1.679 |
| Water related | 0.306 | 0.249 | 1.512 | 0.267 | 1.339 | 0.271 | 0.382 | 0.809 | 1.772 |
| Vegetation | 0.625 | 0.688 | 0.770 | 0.586 | 0.662 | 0.530 | 0.642 | 0.920 | 1.195 |
| Artificial + urban | 1.787 | 1.846 | 6.068 | 1.974 | 4.214 | 1.544 | 1.210 | 3.086 | 4.912 |
| Meadows | 0.165 | 0.191 | 1.969 | 0.197 | 1.177 | 0.176 | 0.113 | 0.725 | 1.757 |

    Urban fabric consistently shows significantly higher Bowen Index values), which suggests a higher ratio of sensible heat flux over sensible heat flux, and the trend is overall varying.

    Due to the lack of in-situ ground data that would allow direct evaluation, we resorted to using third-party data. However, no suitable control data was found for a study of such a small area. Out of the available coarse-scale data, the LSA SAF Data Ser-
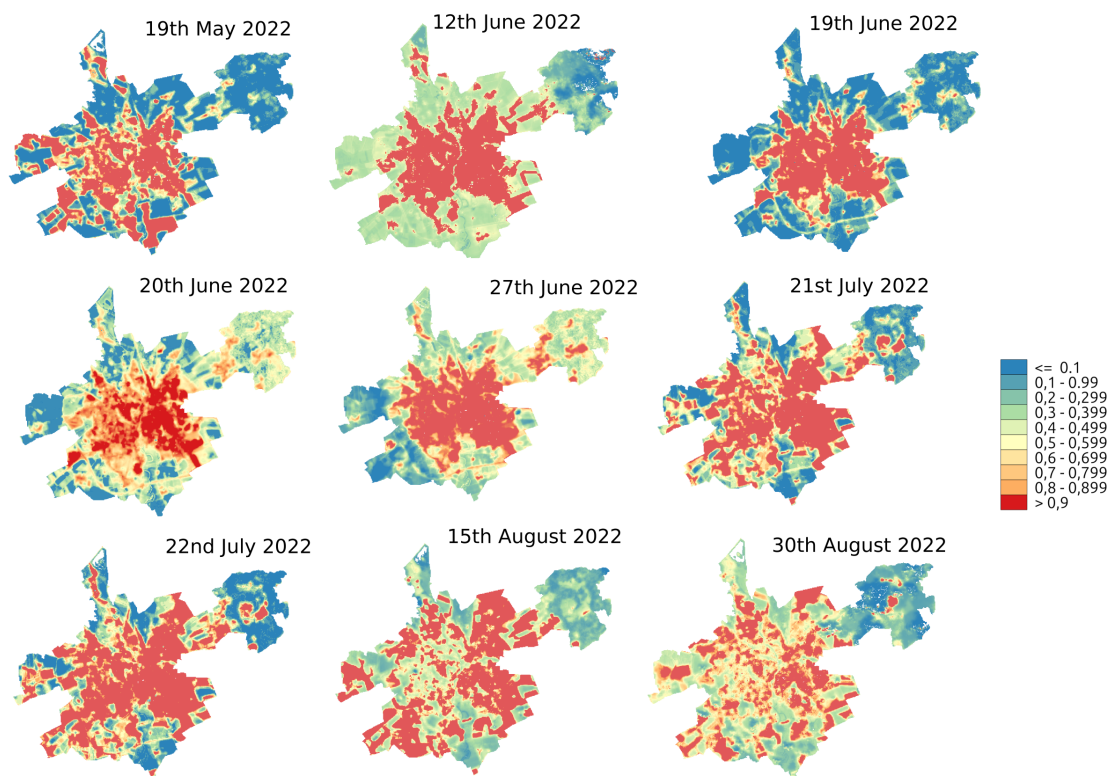
**Figure 9.** Bowen Index Values on areas of habitats through spring and summer 2022.

vice (EUMETSAT) was chosen for the evaluation of sensible and latent heat flux (Table 5) from the Meteosat 2nd Generation. To create matching data, Landsat images used in this study were reprojected (from original EPSG:32633 to EPSG:4326) and resampled (using median resampling) to match the resolution of EUMETSAT data. This created a grid ofd of six times three cells which covered the area of interest.

**Table 5.** Data used for evaluation.

| Acronym | Description | Format | Time | Units | Spatial Resolution |
|---------|-------------|--------|------|-------|--------------------|
| MHv3 | Sensible Heat Flux | netCDF | 09:30 UTC | $W/m^2$ | 0.05 ° |
| LE | Latent Heat Flux | netCDF | 09:30 UTC | $W/m^2$ | 0.05 ° |

Two sensing days were chosen for data evaluation: 22nd July and 15th August.

The averages of Landsat imagery proved to be consistently higher than the averages of EUMETSAT data. The correlation percentages show a mixed pattern. For the 11th May, the correlation of the Bowen Index is negative (see Table 8), uggesting

Hydrology and
Earth System
Sciences
Discussions
Open Access
EGU

**Table 6.** Statistical comparison of data evaluation of Sensible Heat Flux.

|  | Landsat Imagery Avg. [$W/m^2$] | EUMETSAT Evaluation Avg. [$W/m^2$] | Difference [$W/m^2$] | Pearson Correlation [%] |
|---|---|---|---|---|
| 22nd July | 261.78 | 168.38 | 93.40 | 77.46 |
| 15th August | 349.27 | 207.16 | 142.11 | 88.75 |

an inverse relationship. For 22nd July, there is a high positive correlation. The direction of the bias (overestimation or underestimation) in the Landsat Imagery compared to EUMETSAT evaluation is consistent across all three variables (SHF, LHF, BI) and dates.

**Table 7.** Statistical comparison of data evaluation of Latent Heat Flux.

|  | Landsat Imagery Avg. [$W/m^2$] | EUMETSAT Evaluation Avg. [$W/m^2$] | Difference [$W/m^2$] | Correlation [%] |
|---|---|---|---|---|
| 22nd July | 152.05 | 182.0 | 29.94 | 71.15 |
| 15th August | 141.72 | 148.55 | 6.83 | 73.18 |

160    Evaluation is consistent across all three variables (H, LE, BI) and dates. Despite the bias, there is a noticeable correlation between Landsat Imagery and EUMETSAT Evaluation values, indicating a consistent relationship that might be affected by a scaling or offset issue (Tables 6, 7, 8).

**Table 8.** Statistical comparison of data evaluation of Bowen Index.

|  | Landsat Imagery Avg. | EUMETSAT Evaluation Avg. | Difference | Correlation [%] |
|---|---|---|---|---|
| 22nd July | 1.17 | 0.50 | 0.66 | 84.82 |
| 15th August | 1.59 | 0.86 | 0.72 | 71.28 |

## 5   Discussion

The observed Bowen Index values in urban areas, indicating Sensible Heat Flux, agree with highlighting the urban heat island
165    effect Kotthaus and Grimmond (2014). Additionally, the study's identification of lower Bowen Index values in vegetated areas agrees with the established understanding of the cooling effect associated with Latent Heat Flux from vegetation.

The described distinct patterns observed in different land cover classes show the importance of considering land use and/or land cover characteristics in understanding energy exchanges Wang et al. (2019); Pal and Ziaul (2017). The findings have implications for local climate studies.

170    Land Surface Temperature, Albedo, Net Radiation, and Sensible and Latent Heat Flux are pivotal variables, collectively contributing to the Bowen Index — a key metric for understanding energy partitioning in terrestrial systems. In particular, accurately determining these variables is essential for unravelling the Bowen Index. This is why this article applied proven and often used procedures (such as Liang's approach to albedo calculation (Liang, 2001)) or these determinations. Sensible

and Latent Heat Flux are routinely determined using various evapotranspiration models; for this study, we chose the S-SEBI

175    approach for its simplicity.

Despite the challenges associated with spatial and temporal variability in atmospheric conditions, our integration of meteorological data and remote sensing techniques contributed to a comprehensive understanding of the local climate. Moreover, validating our results through a comparison with EUMETSAT evaluation data indicated a consistent relationship, however, with some biases. This suggests the potential reliability of our approach and the robustness of derived heat fluxes and Bowen

180    Index values. The consistent bias direction across multiple variables and dates suggests a potential scaling or offset issue, which could be further investigated and adjusted in future studies. The spatial distribution of Sensible Heat Flux, Latent Heat Flux and Bowen Index is shown through maps, providing a comprehensive understanding of the heterogeneity in the study area..

Comparative analysis with previous research studies becomes challenging due to the predominant utilization of Bowen index values as non-spatial data. The source of these values emerges from flux towers or eddy covariance towers. Furthermore, these

185    values are often used as input data for Heat Flux calculation to determine evapotranspiration. The original Bowen Index values measured during the studies are usually not integrated into results or discussions in other articles. Few studies have shown actual Bowen Index valuess (Jo et al., 2002).

Our study also confirmed the great importance and potential of thermal data for selected environmental studies (Weng, 2009; Alavipanah et al., 2018), but at the same time, had to face the barrier of spatial resolution, which makes it impossible to

190    perform analyses at the level of habitats or small green areas in the city. Still, these areas had to be aggregated or eliminated. Unfortunately, the supply of satellite thermal data is not very large (Segarra, 2024) and it would be very welcome if a future Sentinel mission had a thermal band with high (to very high) spatial resolution.

## 6    Conclusions

In this study, we investigated a part of the Olomouc region's thermal dynamics and energy balance in the northeastern part of

195    the Czech Republic. Using Landsat 8 and Landsat 9 imagery, meteorological data, and advanced algorithms, our research aimed to partly unravel the complex interactions between land cover, net radiation, and heat fluxes during the spring and summer of 2022.

Our findings revealed significant spatial variability in Land Surface Temperature (LST) and albedo, offering valuable insights into the thermal characteristics of the study area. The calculated Solar Net Radiation and subsequent analysis of Sensible and

200    Latent Heat Fluxes provided a nuanced understanding of the energy exchanges occurring at the surface. Applying the S-SEBI algorithm allowed us to determine Bowen Index (BI), highlighting distinct patterns across different land cover classes.

Urban and artificial areas consistently exhibited higher Bowen Index values, indicating a higher sensible heat flux, while areas abundant in vegetation showcased lower BI values, suggesting a dominance of latent heat flux and higher effectivity of evapotranspiration and cooling function of vegetation. Our study further demonstrated the temporal trends in BI, showcasing

205    variations during specific sensing days.

The practical advantage is that the method allows for a fast, iterative and non-destructive solution, which helps to provide results for a large territory. The result is spatial data capturing the time-resolved variability in the monitored territory, which is easily transferable to other areas.

The obtained data can be used in spatial planning, e.g., in mitigation and adaptation measures.

210 *Author contributions.* TP: conceptualization, methodology, writing; VP: conceptualization, methodology, editing

*Competing interests.* The authors have declared no competing interests.

Hydrology and
Earth System
Sciences
Discussions
Open Access
EGU

# References

215   Acharya, B. and Sharma, V.: Comparison of satellite driven surface energy balance models in estimating crop evapotranspiration in semi-arid to arid inter-mountain region, Remote Sensing, 13, 1822, 2021.

Alavipanah, S., Schreyer, J., Haase, D., Lakes, T., and Qureshi, S.: The effect of multi-dimensional indicators on urban thermal conditions, Journal of cleaner production, 177, 115–123, 2018.

Anderson, R. G. and Goulden, M. L.: A mobile platform to constrain regional estimates of evapotranspiration, agricultural and forest meteo-
220   rology, 149, 771–782, 2009.

Avdan, U. and Jovanovska, G.: Algorithm for automated mapping of land surface temperature using LANDSAT 8 satellite data, Journal of sensors, 2016, 1–8, 2016.

Berbers, Y. and Zwaenepoel, W., eds.: Proceedings of 25th Hydro 2020, International Conference, NIT Rourkela, ISBN 978-93-90631-56-8, 2021.

225   Chatterjee, S., Kandiah, R., Watts, D., Sritharan, S., and Osterberg, J.: Estimating Completely Remote Sensing-Based Evapotranspiration for Salt Cedar (Tamarix ramosissima), in the Southwestern United States, Using Machine Learning Algorithms, Remote Sensing, 15, 5021, 2023.

Cho, J., Oki, T., Yeh, P. J.-F., Kim, W., Kanae, S., and Otsuki, K.: On the relationship between the Bowen ratio and the near-surface air temperature, Theoretical and Applied Climatology, 108, 135–145, 2012.

230   Favretto, A. et al.: Urban Heat Island analysis with Remote Sensing and GIS methods: an application in the Trieste area (North-East of Italy), Bollettino Della Società Geografica Italiana Serie, 1, 215–229, 2018.

Held, A., Steduto, P., Orgaz, F., Matista, A., and Hsiao, T.: Bowen ratio/energy balance technique for estimating crop net $CO_2$ assimilation, and comparison with a canopy chamber, Theoretical and Applied Climatology, 42, 203–213, 1990.

Jo, Y.-H., Yan, X.-H., Pan, J., He, M.-X., and Liu, W. T.: Calculation of the Bowen ratio in the tropical Pacific using sea surface temperature
235   data, Journal of Geophysical Research: Oceans, 107, 17–1, 2002.

Kotthaus, S. and Grimmond, C. S. B.: Energy exchange in a dense urban environment–Part I: Temporal variability of long-term observations in central London, Urban Climate, 10, 261–280, 2014.

Law, B. E., Falge, E., Gu, L., Baldocchi, D. D., Bakwin, P., Berbigier, P., Davis, K., Dolman, A. J., Falk, M., Fuentes, J., et al.: Environmental controls over carbon dioxide and water vapor exchange of terrestrial vegetation, Agricultural and Forest Meteorology, 113, 97–120, 2002.

240   Liang, S.: Narrowband to broadband conversions of land surface albedo I: Algorithms, Remote sensing of environment, 76, 213–238, 2001.

Mallick, K., Bhattacharya, B. K., Rao, V., Reddy, D. R., Banerjee, S., Venkatesh, H., Pandey, V., Kar, G., Mukherjee, J., Vyas, S. P., et al.: Latent heat flux estimation in clear sky days over Indian agroecosystems using noontime satellite remote sensing data, Agricultural and Forest Meteorology, 149, 1646–1665, 2009.

Markham, B. L. and Barker, J. L.: Spectral characterization of the Landsat Thematic Mapper sensors, International Journal of Remote
245   Sensing, 6, 697–716, 1985.

Nagler, P. L., Scott, R. L., Westenburg, C., Cleverly, J. R., Glenn, E. P., and Huete, A. R.: Evapotranspiration on western US rivers estimated using the Enhanced Vegetation Index from MODIS and data from eddy covariance and Bowen ratio flux towers, Remote sensing of environment, 97, 337–351, 2005.

Pal, S. and Ziaul, S.: Detection of land use and land cover change and land surface temperature in English Bazar urban centre, The Egyptian
250   Journal of Remote Sensing and Space Science, 20, 125–145, 2017.

Pechanec, V., Cudlín, O., Zapletal, M., Purkyt, J., Štěrbová, L., Chobot, K., Tangwa, E., Včeláková, R., Prokopová, M., and Cudlín, P.: Assessing Habitat Vulnerability and Loss of Naturalness: Applying the GLOBIO3 Model in the Czech Republic, Sustainability, 13, 5355, 2021.

Roerink, G., Su, Z., and Menenti, M.: S-SEBI: A simple remote sensing algorithm to estimate the surface energy balance, Physics and Chemistry of the Earth, Part B: Hydrology, Oceans and Atmosphere, 25, 147–157, 2000.

Sai Krishna, S., Manavalan, P., and Rao, P.: Estimation of net radiation using satellite based data inputs, The International Archives of the Photogrammetry, Remote Sensing and Spatial Information Sciences, 40, 307–313, 2014.

Segarra, J.: Satellite Imagery in Precision Agriculture, in: Digital Agriculture: A Solution for Sustainable Food and Nutritional Security, pp. 325–340, Springer, 2024.

Su, Z.: The Surface Energy Balance System (SEBS) for estimation of turbulent heat fluxes, Hydrology and earth system sciences, 6, 85–100, 2002.

University, P.: Basic Information, Available at https://www.upol.cz/en/university/basic-information/, 2024.

Wang, W., Liu, K., Tang, R., and Wang, S.: Remote sensing image-based analysis of the urban heat island effect in Shenzhen, China, Physics and Chemistry of the Earth, Parts a/b/c, 110, 168–175, 2019.

Weng, Q.: Thermal infrared remote sensing for urban climate and environmental studies: Methods, applications, and trends, ISPRS Journal of photogrammetry and remote sensing, 64, 335–344, 2009.

Weng, Q., Lu, D., and Schubring, J.: Estimation of land surface temperature–vegetation abundance relationship for urban heat island studies, Remote sensing of Environment, 89, 467–483, 2004.

Wilson, K. B., Baldocchi, D. D., Aubinet, M., Berbigier, P., Bernhofer, C., Dolman, H., Falge, E., Field, C., Goldstein, A., Granier, A., et al.: Energy partitioning between latent and sensible heat flux during the warm season at FLUXNET sites, Water Resources Research, 38, 30–1, 2002.

Wylie, B. K., Johnson, D. A., Laca, E., Saliendra, N. Z., Gilmanov, T. G., Reed, B. C., Tieszen, L. L., and Worstell, B. B.: Calibration of remotely sensed, coarse resolution NDVI to CO2 fluxes in a sagebrush–steppe ecosystem, Remote Sensing of Environment, 85, 243–255, 2003.

ČÚZK, ČSÚ, and ARCDATA, P.: Data ArcČR ©, Available at https://www.arcgis.com/home/item.html?id= 16fd9804dac04020938452a77c1ed350, 2023.